Real-time detection of PRT1-mediated ubiquitination via fluorescently labeled substrate probes

Augustin C. Mot,[1,2,4] Erik Prell,[3,5] Maria Klecker,[1,2] Christin Naumann,[1,2] Frederik Faden,[1,2] Bernhard Westermann[3] & Nico Dissmeyer[1,2,*]

[1] Independent Junior Research Group on Protein Recognition and Degradation, Leibniz Institute of Plant Biochemistry (IPB), Weinberg 3, D-06120 Halle (Saale), Germany

[2] ScienceCampus Halle – Plant-based Bioeconomy, Betty-Heimann-Str. 3, D-06120 Halle (Saale), Germany

[3] Department of Bioorganic Chemistry, Leibniz Institute of Plant Biochemistry (IPB), Weinberg 3, D-06120 Halle (Saale), Germany

[4] present address: Faculty of Chemistry and Chemical Engineering, Babes-Bolyai University, 11 Arany Janos, Cluj-Napoca, Romania

[5] present address: Max Planck Institute for Biophysical Chemistry, Am Fassberg 11, D-37077 Göttingen, Germany

[*] Correspondence should be addressed to N.D. (nico.dissmeyer@ipb-halle.de).

RUNNING TITLE

Live assays with fluorescent N-end rule substrates

KEY WORDS

activity profiling, labeling chemistry, protein labeling, fluorescence polarization, fluorescent dyes, fluorescent substrates, compound library screening, fluorophoric halooacetamides

29 **ABSTRACT**

30 **The N-end rule pathway has emerged as a major system for controlling protein sta-**
31 **bility in medical, animal and plant sciences as well as agriculture. This included the**
32 **discovery of novel functions and enzymes of the pathway. Ubiquitination mechanism**
33 **and substrate specificity of *bona fide* N-end rule pathway E3 Ubiquitin ligases is still**
34 **elusive. Taking the first discovered *bone fide* plant N-end rule E3 ligase PROTEOLY-**
35 **SIS1 (PRT1) as a model, we describe a novel tool to molecularly characterize**
36 **polyubiquitinylation live, in real-time. We demonstrate that PRT1 is indeed an E3**
37 **ligase and gain mechanistic insights in PRT1 substrate preference and activation by**
38 **monitoring live ubiquitination by using a fluorescent chemical probe coupled to arti-**
39 **ficial substrate reporters. Ubiquitination can then be measured by rapid in-gel fluo-**
40 **rescence scanning in classical end-point assays as well as in real time by fluores-**
41 **cence polarization in standard microplate readers. Enzymatic activity, substrate**
42 **specificity, reaction mechanisms and optimization can be easily investigated *ad hoc***
43 **in short time and with significantly reduced reagent consumption.**

44 **INTRODUCTION**

45 The ON/OFF status of proteins within the cells' proteome, their general abundance
46 and specific distribution throughout the compartments and therefore their functions and
47 activities are precisely controlled by protein quality control (PQC) mechanisms to ensure
48 proper life of any organism. Therefore, the biochemical analysis of the underlying mecha-
49 nisms safeguarding proteostatic control is pivotal. It ranges from the molecular characteri-
50 zation of enzymes involved in PQC and their catalyzed reactions to enzyme-substrate to
51 non-substrate protein-protein interactions. The so-called Ubiquitin (Ub) 26S proteasome
52 system (UPS) is a master component of PQC with the central core units of non-catalytic Ub
53 ligases (E3), the Ub-conjugating enzymes (E2), and the Ub-activating enzymes (E1).

54 To investigate an element conferring substrate specificity, we chose PROTEOLYSIS1
55 (PRT1) as a model E3 ligase, which is a *bona fide* single-subunit E3 with unknown substrate
56 portfolio.[1-3] Its biological function remains elusive but it presumably represents a highly
57 specific enzyme of the N-end rule pathway of targeted protein degradation, which is a part
58 of the UPS. The N-end rule relates the half-life of a protein to its N-terminal amino acid[4] and
59 causes rapid proteolysis of proteins bearing so-called N-degrons, N-terminal sequences
60 that lead to the degradation of the protein. N-degrons are created by endoproteolytic
61 cleavage of protein precursors (pro-proteins) and represent the resulting neo-N-termini of
62 the remaining C-terminal protein moiety, albeit not all freshly formed N-termini automati-
63 cally present destabilizing residues (**Figure 1a**).

64 The N-end rule pathway is an emerging vibrant area of research and has a multitude
65 of functions in all kingdoms.[5-9] Identified substrates are mainly important regulatory pro-

teins and play key roles in animal and human health,[10-14] plant stress response and agriculture.[9, 15-20]

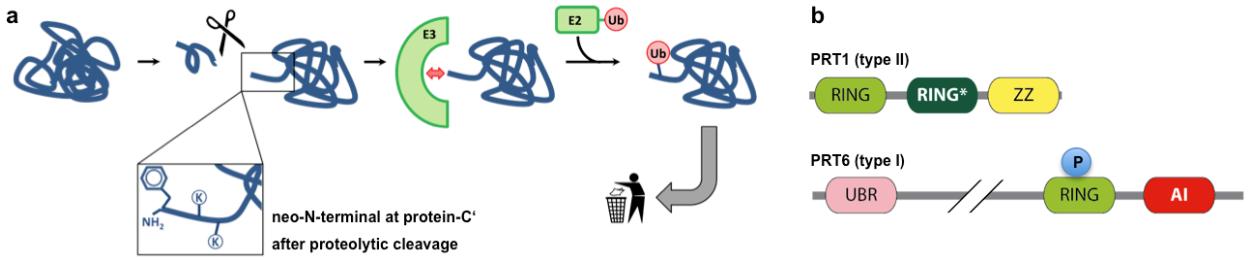

Figure 1. Generation of N-end rule substrates by proteolytic processing and predicted features of the two *bone fide* plant N-recognins. a) Substrates containing N-degrons can be generated from (pre-)pro-proteins as precursor sequences after proteolytic cleavage (indicated by the scissors). The N-degron shown here comprises a Phe residue as primary destabilizing residue at the protein-C' and internal lysines for polyubiquitination. These N-degrons can be recognized by N-end rule E3 Ub ligases (N-recognins) which in turn associate with Ub-conjugating enzymes (E2) carrying Ub which was previously activated by E1 enzymes. One possible result of ubiquitination is protein degradation and to date, in the context of the N-end rule, ubiquitination is assumed to lead to degradation in most of the cases. **b)** The two known *Arabidopsis* N-recognins were identified by their function (PRT1, 46 kDa) and by homology to the UBR-box from *S. cerevisiae* UBR1p (PRT6, 224 kDa). UBR: box binding type I substrates; RING*: composite domain containing RING and CCCH-type Zn fingers; ZZ: Zinc binding domain similar to RING; RING: protein-protein interaction domain for E2–E3 interaction; AI: predicted autoinhibitory domain (intramolecular interaction); P: phosphorylation site (PhosPhAt 4.0; phosphat.uni-hohenheim.de). b is modified from Tasaki et al., 2012.

In plants, functions of N-end rule enzymes are associated with central developmental processes including seed ripening and lipid breakdown, hormonal signaling of abscisic acid (ABA), gibberellin and ethylene, with seed dormancy and germination,[21-23] with leaf and shoot morphogenesis, flower induction, and apical dominance,[24] and the control of leaf senescence.[25] Then, the pathway was shown to be a sensor for reactive oxygen species (ROS) by mediating nitric oxide (NO) signaling and regulating stress response after hypoxia, e.g. after flooding and plant submergence.[15-17] A novel plant-specific class of enzymes was associated with the pathway, i.e. plant cysteine oxidases (PCOs), highlighting plant-specific molecular circuits, enzyme classes and mechanisms.[18] In the moss *Physcomitrella patens*, N-end rule mutants are defective in gametophytic development[26] and protein tar-

93 gets of N-end rule-mediated posttranslational modifications were discovered.[27] Also in bar-
94 ley, the pathway is connected with development and stress responses.[19] Only very recently,
95 a link between N-end rule function and plant-pathogen response and innate immunity was
96 found,[20] shedding light on novel functions of the yet underexplored branch of targeted pro-
97 teolysis. However, to date, the identity of plant N-end rule targets still remains obscure and
98 clear evidences from biochemical data of *in vitro* and *in vivo* studies such as N-terminal
99 sub-proteomics or enzymatic assays are still lacking.

100 A novel *in vivo* protein stabilization tool for genetic studies in developmental biology
101 and biotechnological applications, the 'lt-degron', works in plants and animals by directly
102 switching the levels of functional proteins *in vivo*.[28] The method is based on conditional and
103 specific PRT1-mediated proteolysis, the process studied in depth with the here-generated
104 fluorescent substrate reporters.

105 N-degrons are by definition recognized and the corresponding protein ubiquitinated
106 by specialized N-end rule E3 ligases, so-called *N-recognins*.[5, 7, 8, 29] In plants, only two of the-
107 se, namely PRT1 and PRT6, are associated with the N-end rule (**Figure 1b**). This is in con-
108 trast to the high number of proteolytically processed proteins which carry in their mature
109 form N-terminal amino acids that could potentially enter the enzymatic N-end rule path-
110 way cascade.[30] In the light of more than 800 putative proteases in the model plant *Ara-*
111 *bidopsis thaliana*, it is likely that the N-end rule pathway plays an important role on the
112 half-lives of these protein fragments in a proteome-wide manner. Examples are found in
113 the METACASPASE9 degradome, i.e. that part of the proteome which is associated with
114 degradation,[31] or the N-degradome of *E. coli*[32] with a possibly analogous overlap with en-
115 dosymbiotic plant organelles.[33]

116 PRT1, compared to the *Saccharomyces cerevisiae* N-recognin Ubr1 (225 kDa), is a
117 relatively small protein (46 kDa) and totally unrelated to any known eukaryotic N-
118 recognins but with functional similarities to prokaryotic homologs (**Figure 1b**). It is there-
119 fore perceived as a plant pioneer E3 ligase with both diversified mechanistics and function.
120 Artificial substrate reporters with N-terminal phenylalanine were shown to be stabilized in
121 *prt1* mutant cells.[1-3] However, until today, there are neither *in vivo* targets nor direct func-
122 tions associated with PRT1, however, very recently, a potential role of PRT1 in plant innate
123 immunity was flagged.[20]

124 The spectrum of N-termini possibly recognized by plant N-end rule E3 ligases in-
125 cluding PRT1 is not sufficiently explored. Only Phe-starting test substrates were found to
126 be stabilized in a *prt1* mutant whereas initiation by Arg and Leu still caused degradation.[2, 3,
127 34] However, PRT1 was shown to destabilize also Tyr- and Trp-starting reporter proteins in
128 a heterologous system in *S. cerevisiae*.[3] In the light of substrate identification, it is cardinal
129 to determine PRT1 mechanistics in more detail because several posttranslationally pro-
130 cessed proteins bearing Phe, Trp and Tyr at the neo-N-termini were found[30, 31] and hence
131 represent putative PRT1 targets altogether. Elucidating the substrate specificity of PRT1
132 will be an important step forward towards substrate identification and association of PRT1
133 and the N-end rule with a biological context.

134

135 We established a technique that allows real time measurements of ubiquitination
136 using fluorescence scanning of SDS-PAGE gels and fluorescence polarization. We propose
137 its use as a generic tool for mechanistic and enzymological characterization of E3 ligases as
138 master components of the UPS directing substrate specificity. With a series of artificial test

139 substrates comprising various *bona fide* destabilizing N-end rule N-termini, substrate spec-
140 ificity was analyzed and revealed PRT1 preference for Phe as a representative of the bulky
141 hydrophobic class of amino acids. The *in vitro* ubiquitination methods used so far are based
142 on end-time methods where the reaction is stopped at a given time point and analyzed by
143 SDS-PAGE followed by immunostaining with anti-Ub versus anti-target specific antibodies.
144 This detection via western blot often gives rise to the characteristic hallmark of polyubiqui-
145 tinylated proteins, a "ubiquitination smear" or a more distinct "laddering" of the posttrans-
146 lationally Ub-modified target proteins. All the information of what occurred during the time
147 of reaction is unknown unless the assay is run at several different time points which drasti-
148 cally increases both experimental time and reagent consumption. Existing fluorescence
149 polarization measurements are more frequently used to characterize enzyme-substrate or
150 protein-protein interactions rather than enzyme activity and parameters affecting the per-
151 formance of the ubiquitination reaction.[35-37] To our knowledge, there are no protocols
152 available to monitor substrate ubiquitination in a time-resolved and live manner.

153 We then established a corresponding method that monitors this very process live, in
154 real time, using fluorescently labeled substrate proteins and fluorescence-based detection
155 assays, namely fluorescence polarization. In addition, the protocol was coupled to fast and
156 convenient scanning fluorescence in-gel detection. This type of assay can be easily adapted
157 for high-throughput measurements of ubiquitination and probably also similar protein
158 modification processes involving changes in substrate modification over time *in vitro*.

159

160 Here, we report a novel advanced approach to molecularly characterize E3 ligases,
161 to measure and track polyubiquitination live and in a time-resolved manner. It has the po-

162 tential to lead to profound implications for our understanding of the interactions of E3 lig-
163 ases with substrates and non-substrates and can impact ubiquitination research in general
164 as our work suggests to be transferable to other E3 ligases and enzyme-substrate pairs.
165 The method relies on rapid, easy and cheap protocols which are currently lacking for in-
166 depth biochemical analysis of E3 ligases and is at the same time non-radioactive, sterically
167 not interfering, and works with entire proteins in form of directly labeled substrates.

168 So far, only three reports mention work on PRT1 at all, i.e. the two first brief de-
169 scriptions[2, 3] and one highlighting the role of the N-end rule pathway, in particular a novel
170 function for PRT1, in plant immunity.[20] However, to date, the community lacks proofs
171 demonstrating that PRT1 and other E3 candidates are indeed involved in substrate protein
172 ubiquitination. To date, ubiquitination activities of E3 ligase candidates from the plant N-
173 end rule pathway were only speculated. Here, we demonstrate for the first time that PRT1
174 is indeed involved in polyubiquitination of substrate proteins depending on its N-terminal
175 amino acid.

176

177 **RESULTS AND DISCUSSION**

178 **PRT1 is an E3 ubiquitin ligase and prefers bulky N-termini**

179 For the analysis of PRT1 E3 ligase function, i.e. recognition of N-end rule substrates,
180 we used recombinant PRT1 together with generic substrate reagents with unprecedented
181 detection features combining chemically synthesized fluorophores and recombinant ubiq-
182 uitination acceptors which were used as live protein modification detectors. To describe N-
183 terminal amino acid specificity of PRT1, the N-terminally variable protein parts of the re-
184 porters were engineered as N-terminal His8:MBP fusions comprising a recognition se-

185 quence of tobacco etch virus (TEV) protease at the junction to the subsequent generic sub-
186 strate protein moiety (**Figure 2a, Supplementary Figure 1a**). Cleavage by TEV gave rise
187 to small C-terminal fragments of the His8:MBP-substrate fusions of which the neo-N-
188 terminal, i.e. the P1' residue of the TEV cleavage site, can be altered to all proteinogenic
189 amino acids except proline.[38-40] For a novel fluorescence-based approach, we covalently
190 coupled a synthetic fluorescent probe (**Figure 2b**) to the artificial substrate protein. The
191 resulting reagent serves as fluorescent protein Ub acceptor in N-end rule ubiquitination
192 assays. The architecture of the reagent is as follows: after the cleavable His8:MBP tag, eK, a
193 part of *E. coli* lacZ[4] followed by a triple hemagglutinin epitope tag (3HA) for immunodetec-
194 tion and an *E. coli* flavodoxin (Flv) were combined. Flv was chosen as a highly soluble and
195 stable protein. The junctions between His8:MBP and eK encode for the N-termini glycin
196 (Gly, G), phenylalanin (Phe, F), arginine (Arg, R), and leucin (Leu, L) that get N-terminally
197 exposed after TEV cleavage. The G/F/L/R-eK-Flv constructs contain a single cysteine
198 (Cys101 of Flv) that allowed the labeling of the purified recombinant fusion protein with a
199 novel thiol-reactive probe that comprises a iodoacetamide-polyethylene glycol (PEG) linker
200 and the fluorogenic subunit of 4-nitro-2,1,3-benzoxadiazole (NBD; **Figure 2b**). We chose
201 the latter due to its small size compared to other labeling reagents such as large fluorescein
202 moieties and because it can be detected very specifically by both UV absorption and UV
203 fluorescence with low background interferences.

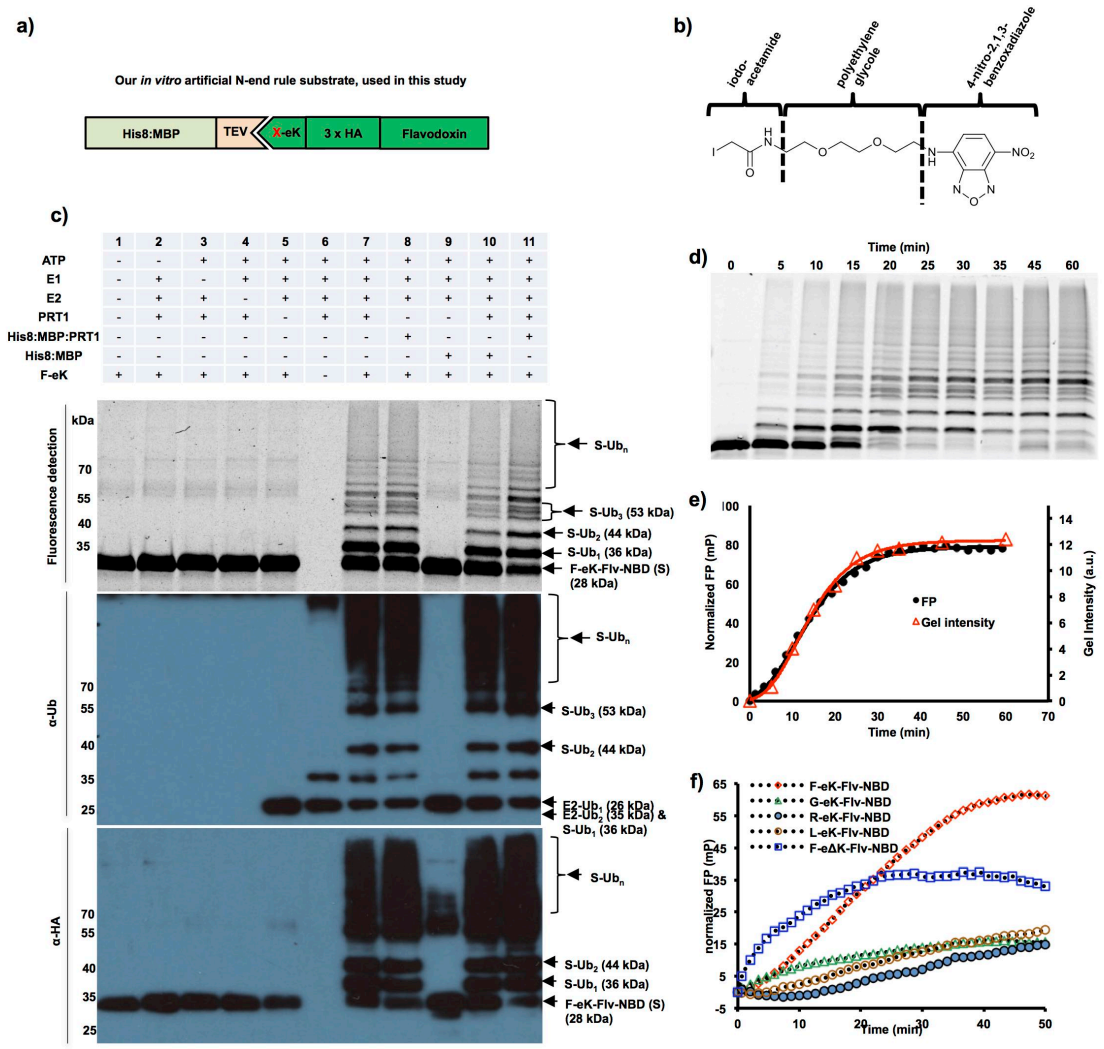

Figure 2. Fluorescent protein conjugates for monitoring *in vitro* substrate ubiquitination in real time. a) Design of recombinant fusion proteins used as N-end rule substrates. After TEV cleavage and removal of the His8:MBP affinity tag, the artificial substrate based on *E. coli* flavodoxin (Flv) is initiated with a neo-N-terminal, here Phe (F), Gly (G), Leu (L) or Arg (R). **b)** Skeletal formula of the synthesized thiol-reactive fluorescent compound. The substrate was covalently tagged with the reagent composed of iodoacetamide, polyethylene glycol (PEG) linker and 4-nitro-2,1,3-benzoxadiazole (NBD). The reactive iodine-containing group on the left couples to the thiol group of internal Cys residues of Flv. NBD serves as a fluorophore with excitation at 470 nm and emission at 520 nm. **c)** Detection via fluorescence and immunoblotting of the F-eK-Flv-NBD after *in vitro* ubiquitination. The labeled protein and its ubiquitinated variants were detected via fluorescence scanning directly from the SDS-PAGE gel followed by western blotting and immunodetection with anti-HA and anti-Ub antibodies. Lane 6 shows autoubiquitination of PRT1 at about 35 kDa and very high molecular weight. Cleaved PRT1 as well as His8:MBP-tagged PRT1 were used together with His:UBA1 (E1) and His:UBC8 (E2).[41] **d and e)** Kinetic profiles of PRT1-mediated ubiquitination. F-eK-Flv-NBD ubiquitination was monitored by FP and in-gel fluorescence scanning. The S-shaped kinetic curve is observed in both in-gel fluorescence scanning detection and fluorescence polarization. **f)** N-terminal specificity evaluated by real-time ubiquitination detection. Fluorescently labelled R-eK-Flv, L-eK-Flv, G-eK-Flv, F-eΔK-Flv and F-eK-Flv were comparatively evaluated for their degree of ubiquitination by PRT1.

221 In an *in vitro* ubiquitination assay, we used recombinant UBC8 as a promiscuous E2
222 conjugating enzyme and UBA1 as E1 activating enzyme[41] and show here for the first time
223 E3 ligase activity of PRT1 depending on E1, E2 and ATP (**Figure 2c**). PRT1 discriminates a
224 substrate by its N-terminal, aiding the transfer of Ub to the substrate and leading to
225 polyubiquitination. Similar assays are evaluated based on immunochemical and colorimet-
226 ric detection, incorporation of radioisotopes such as ^{125}I or ^{32}P, or fluorescently labeled
227 native or recombinant Ub. After immunostaining with anti-Ub antibodies, usually, a typical
228 smear of higher molecular weight compared to the target protein's size is observed or after
229 probing with target-specific antibodies, a more or less distinct laddering, also of high mo-
230 lecular weight, becomes evident. These are the common signs for polyubiquitination and a
231 clear laddering was also visualized by fluorescent scanning in our novel approach. We iden-
232 tified distinct subspecies via in-gel detection (**Figure 2c**). However, in this experimental
233 setup, our assay can be evaluated immediately and gel-based after SDS-PAGE rendering
234 protein transfer via western blotting plus the subsequent steps of blocking, immuno- and
235 chemical detection obsolete.

236 A classical end-time point assay where the reaction was stopped at different reac-
237 tion time points followed by SDS-PAGE and in-gel fluorescence detection revealed the ki-
238 netics of PRT1 activity using F-eK-Flv as substrate (**Figure 2d**). However, a real-time moni-
239 toring of the kinetic profile of the enzymatic reaction is only possible via fluorescence po-
240 larization (FP) in live detection measurements.

241 The protocol described in the following is rapid, non-radioactive, uses only a small
242 fluorophore as covalent dye, works with full substrate proteins instead of only peptides,
243 and can be read out live and in real-time. Moreover, the FP approach conveys superimpos-

244 able kinetic curves with data from classical end-time point assays, but faster, with higher
245 resolution in time and using fewer reagents (**Figure 2e**). The kinetic profile is best-fitted
246 with an S-shaped curve and a growth curve model of logistic type (Richards' equation) ra-
247 ther than exponentially as expected for simple kinetics. A possible explanation for the S-
248 shaped kinetic curve and the presence of an initial lag phase in an increase of the affinity of
249 PRT1 for the monoubiquitinated substrates compared to the non-ubiquitinated population.
250 Preferences of E2s and E3s for mono- or polyubiquitinated substrates and their influence
251 on ubiquitination velocity but also that initial ubiquitination greatly enhances the binding
252 affinity of E3s to the substrate in subsequent reactions was shown previously.[42, 43] Thus,
253 the chain elongation (Ub-Ub isopeptide bond formation) is faster than the chain initiation
254 which might represent the rate limiting-step of the reaction, rather than an E1-E2-
255 controlled limiting-step, see below. Thus, the chain elongation and chain initiation steps
256 appear to be distinct processes that have distinct molecular requisites in agreement with
257 previous findings.[44, 45] The lag phase is reduced if the rate is increased by higher concentra-
258 tion of PRT1.

259 It was previously suggested that PRT1 binds to N-degrons carrying bulky destabiliz-
260 ing residues.[3] By changing the N-terminal residue of the X-eK-Flv-NBD substrate, it was
261 possible to reveal that PRT1 indeed discriminates the substrates according to the N-
262 terminal residue, as expected (**Figure 2f, Supplementary Figure 1b,c**). While the sub-
263 strates carrying G-, R-, L-initiated N-termini showed poor ubiquitination, F-eK-Flv-NBD was
264 heavily ubiquitinated. Additionally, the FP-based assay reveals that the kinetic profile of the
265 ubiquitination is dependent on the position and availability of lysines as Ub acceptor sites
266 as suggested as a characteristic of the N-degrons tested.[46] While the eK-based substrate

267 showed the kinetic curve discussed above, the control F-eΔK-Flv substrate with mutated
268 lysines (expected site of ubiquitination, Lys15 and Lys17, both replaced by Arg) presented
269 a faster initial rate of ubiquitination but levels of only half of the final FP value (**Figure 2f**).
270 This is in good agreement with the in-gel fluorescence detection where lower degrees of
271 ubiquitination of F-eΔK-Flv, reduced mono- and di- ubiquitination - but still clear polyubiq-
272 uitination - were observed (**Supplementary Figure 1c**). This suggested that by lowering
273 the overall number of available lysines in the substrate (two Lys less than in X-eK-Flv con-
274 structs with 11 Lys in total) the overall ubiquitination was detectably reduced. However,
275 this simple end-point assay could not unravel if this was due to altered velocity of chain
276 initiation versus chain elongation. But the initiation per Lys residue was expected to be
277 similar in eK- versus eΔK-Flv substrates but chain elongation could apparently start faster
278 in F-eΔK-Flv. This demonstrates that the presences of E2 together with the particular sub-
279 strate play key roles in the formation of the molecular assembly facilitating the ubiquitina-
280 tion process. Already the intermolecular distance between the E3 ligase and the Ub accep-
281 tor lysines of the substrate as well as the amino acid residues proximal to the acceptor ly-
282 sines determine the progress of the reaction and ubiquitination specificity.[42] Taking the
283 slower initiation of polyubiquitination of F-eΔK-Flv into account, the availability of lysines
284 at the N-terminus might interfere with the monoubiquitination of other, more distal lysines
285 and the E3 could remain associated with substrates that are monoubiquitinated at the N-
286 terminal.

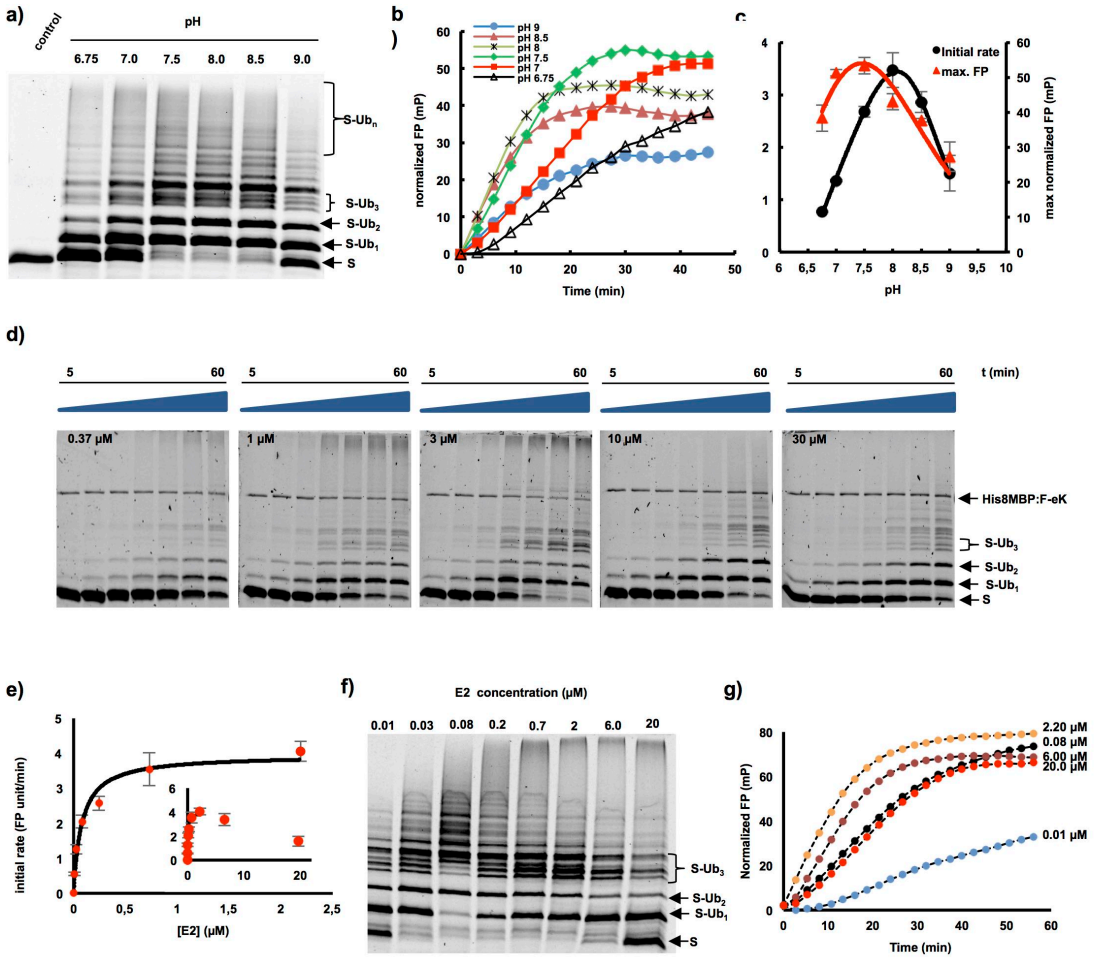

Figure 3. Applications of fluorescent protein conjugates for monitoring pH dependent ubiquitination and enzymatic parameters of PRT1 E3 ligase. a-c) pH dependent ubiquitination of the F-eK-Flv substrate. **a)** In-gel detection of F-eK-Flv ubiquitinated species after 1 h reaction at several pH values demonstrating different patterns of polyubiquitination preferences depending on the pH. **b)** Kinetic profiles, **c)** initial rates and maximum end-time FP values forming a bell-shaped distribution depending on the pH. **d-g)** PRT1-mediated ubiquitination of F-ek-Flv dependent on the concentration of E2-conjugating enzyme (UBC8). **d)** Time dependence of ubiquitination at several E2 concentrations for the first 60 min at 5 nM PRT1, time scale: 5-60 min. **e)** Michaelis-Menten curve plotted using the initial rate from FP data suggest an E2-driven inhibition effect. **f)** The qualitative evaluation of ubiquitination was done using in-gel scanning fluorescence and **g)** kinetic profiles were obtained using FP measurements, similar conditions as in d) but with ten times higher concentration of PRT1, i.e. 50 nM.

299 Another remarkable observation of the ubiquitination pattern in the in-gel fluores-
300 cence image (using three different independent substrate protein purifications of F-eK-Flv-
301 NBD) is that the tri-ubiquitinated form presents three distinct subspecies which eventually
302 lead to a multitude of other species at higher level (**Supplementary Figure 1b**). This could
303 be explained by the possible formation of various ubiquitinated isoforms of the substrate
304 fusion protein generated by utilizing different lysine side chains as ubiquitination acceptor
305 sites. These could be either within the sequence of eK (e.g. Lys15 and Lys17) or within Flv
306 (e.g. Lys100 and Lys222 which seem structurally more favored according to the structural
307 model, **Supplementary Figure 1a**). This is further supported by the fact that there is only
308 one species of tri-ubiquitinated F-eΔK-Flv-NBD, where two ubiquitination acceptors sites
309 within eK (Lys15 and Lys17) were replaced by Arg (**Supplementary Figure 1b**).

310

311 **Fluorescently labeled substrate proteins unravel mechanism of PRT1-mediated**
312 **ubiquitination**

313 The combination of the proposed two fluorescence-based methods allowed fast and
314 efficient *in vitro* investigation of the ubiquitination process via the E3 ligase PRT1 and the
315 optimization of the reaction conditions. In terms of applications, the kinetic approach al-
316 lows collecting data that can assist to easily set up high-throughput assays by checking di-
317 verse variables in short time, e.g. for screens of inhibitors and small molecules potentially
318 facilitating or enhancing ubiquitination. In our example, this included testing of the enzy-
319 matic parameters of E2-E3 interactions and substrate specificities for PRT1. Similar ap-
320 proaches have used labeling with radionuclides or fluorescent dyes coupled to Ub.[47] The
321 latter covalent modification of Ub with fluorescent moieties is often impractical since these
322 groups can sterically hinder the E1-catalyzed activation and E2-dependent transthiolation

323 reactions.[48] This in turn can alter the rate-limiting step. The use of radioactive isotopes re-
324 quires at least running an SDS-PAGE and gel-drying or western blotting followed by auto-
325 radiography for hours to days.
326
327 ***Influence of the pH on PRT1 function as E3 ubiquitin ligase***
328 As a first approach utilizing the real-time assay in the context of substrate ubiquiti-
329 nation, we studied the role of changes in pH on the ubiquitination process mediated by
330 PRT1. A classical end-time approach revealed the reaction optimum to be clearly above pH
331 7 but below pH 9 as indicated by the occurrence of polyubiquitinated species of the fluo-
332 rescent substrate probe F-eK-Flv-NBD (**Figure 3a**). However, using our real-time FP proto-
333 col, we additionally acquired the kinetic profile of the PRT1-mediated ubiquitination pro-
334 cess (**Figure 3b**) and the maximum reached polarization values of this reaction (**Figure**
335 **3c**). These correlated with the amount of polyubiqutinated species detected in the SDS-
336 PAGE gel-based end-time experiment (**Figure 3a**) and the highest initial rate (**Figure 3c**)
337 whereas the latter appears to be different from the reaction optimum according to the de-
338 tected max. FP. We also had previously obvserved, that F-eΔK-Flv ubiquitination presented
339 a faster initial rate but only half of the final FP (**Figure 2f**) and lower degrees of final ubiq-
340 uitination (**Supplementary Figure 1c**). Both bell-shaped forms of the pH dependence for
341 the highest initial reaction rate (pH 8.0) and the maximum substrate polyubiquitination
342 rate (pH 7.5) indicate two competing processes that generate a local maximum (**Figure 3c**).
343 In the light of recently discussed mechanisms of E3 ligase action[49] and the predicted two
344 RING domains of PRT1,[3] higher ubiquitination rates with increased pH can be due to depro-
345 tonation of the attacking lysine side chain of the E2 active site. This facilitates thioester

346 cleavage between E2 and Ub and thereby mediates Ub transfer to the substrate lysine(s),
347 an effect similar to the influence of the acidic residues in close vicinity of the E2 active site,
348 which also cause deprotonation of the lysine side chain of the incoming substrate.[50] This
349 possibly explains the drastic increase in the initial rate of PRT1 substrate ubiquitination in
350 the pH 6.8 to pH 8 range (**Figure 3c**). The competing processes leading to the decrease in
351 ubiquitination at pH>8 could be destabilization of ionic and hydrogen bonds at alkaline pH
352 simply interfering with protein-protein interaction or ATP hydrolysis affecting the Ub
353 charging of the E2 by the E1. This could also explain the premature leveling of the kinetic
354 curves in the FP measurements at pH>8 (**Figure 3b**) while in a longer reaction timescale,
355 the maximum FP values would be expected to be the same at pH 6.8 to pH 7.5.
356
357 ***Interaction of E3 ligase PRT1 with E2-conjugating enzymes***
358 A strong decrease of the ubiquitination rate mediated by PRT1 was observed at
359 higher concentrations of the E2-conjugating enzyme UBC8 (>2 μM) both via in-gel fluores-
360 cence (**Figure 3d**) and FP (**Figure 3e-g**). Based on the FP measurements using up to 2 μM
361 of UBC8, the K_M of substrate ubiquitination by PRT1 at different E2 concentrations was
362 found to be in the submicromolar range, 0.08±0.01 μM, indicating a very tight binding of
363 the E2 to PRT1 compared to other RING E3 ligases[51] (**Figure 3e**). The apparent catalytic
364 rate constant (k_{cat}) of the Ub transfer, i.e. the rate limiting step, was found to be 1.30±0.07 s^{-}
365 ^{1}, which suggests that PRT1 has a high turnover number due to a highly active catalytic cen-
366 ter. Moreover, the distribution pattern of the ubiquitinated substrate species at the end of
367 the reaction (**Figure 3f**) and the kinetic profiles of ubiquitination (**Figure 3g**) are different,
368 depending on the used E2 concentration. This suggests that the E2 concentration does not

369 only influence the rate of the Ub transfer to the substrate but also the mechanism itself.
370 Possible causes are the two separate and potentially distinctly favored chain initiation and
371 elongation processes mentioned above. These could result in lowering the rate of the initia-
372 tion step at higher E2 concentrations since both the kinetic profile and the formation of
373 ubiquitinated species are affected and also the attacking lysines could be structurally dif-
374 ferently favored. This is especially suggested by the variable occurrence of the distinct pat-
375 tern of triubiquitinated substrate species (**Figure 3d,f**) as mentioned above and discussed
376 in other systems as well.[51]
377

378 **MATERIAL AND METHODS**

379 ***Cloning and expression of recombinant proteins***

380 *Artificial N-end rule substrates*

381 *Escherichia coli* flavodoxin (Flv, uniprot ID J7QH18) coding sequence was cloned directly
382 from *E. coli* DNA BL21(DE3) and flanked by an N-terminal triple hemagglutinin (HAT)
383 epitope sequence using the primers Flv_rvs (5‘-TTATTTGAGTAAATTAATCCACGATCC-3‘)
384 and Flv_eK_HAT(oh)_fwd (5‘-CTGGTGCTGCAGATATCACTCTTATCAGCGG-3‘). The X-eK se-
385 quences comprising codons for various N-terminal amino acids exposed after TEV cleavage
386 of the expressed X-eK-Flv fusion protein were cloned from an eK:HAT template using the
387 primers eK(X)_TEV(oh)_fwd (5’-GAGAATCTTTATTTTCAGxxx CACGGATCTGGAGCTTG-3’
388 with xxx=GTT (for Phe), GGG (for Gly), GAG (for Arg), and GTT (for Leu)) and
389 eK_HAT_flav(oh)_rvs (5’-CCGCTGATAAGAGTGATATCTGCAGCACCAG-3’). This sequence
390 contains a TEV protease recognition sequence (ENLYFQ|X with X being the neo-N-terminal
391 after cleavage, i.e. TEV P1' residue) at the N-terminal of the expressed X-eK-Flv fusion pro-

392 tein. In order to attach Gateway attB sites and fuse the PCR products, a PCR was performed
393 using Flv_attB2(oh)_rvs (5'-GGGACCACTTTGTACAAGAAAGCTGGGTA TCATTATTTGAG-
394 TAAATTAATCCACGATCC-3') and adapter_tev_fwd (5'-GGGGACAAGTTTG TACAAAAAA-
395 GCAGGCAGGCTTAGAAAACCTGTAT TTTCAGGGAATG-3'). All primer sequences are listed in
396 **Supplementary Table 1**. An LR reaction into pVP16[52] (kind gift from Russell L. Wrobel,
397 University of Wisconsin-Madison) lead to the final construct that consists of an N-terminal
398 8xHis:MBP double affinity tag. The expression vector pVP16::8xHis:MBP:tev:eK:3xHA:Flv
399 was transformed into *E. coli* BL21(DE3) and the fusion protein was expressed by 0.2 mM
400 IPTG induction in LB medium for 16 h at 26°C. Cells were harvested via centrifugation
401 (3,500 g, 4°C, 20 min), resuspended in Ni-buffer (50 mM sodium phosphate pH 8.0, 300 mM
402 NaCl), treated with 1mg/mL lysozyme (Sigma) in the presence of PMSF (Santa Cruz Bio-
403 technology, sc-3597) added to a final concentration of 1 mM followed by sonication (4 min
404 40 %, 6 min 60% intensity). The lysate was centrifuged (12,500 g, 30 min), the supernatant
405 loaded onto a Ni-NTA agarose column (Qiagen) equilibrated with Ni-buffer, followed by Ni-
406 buffer washing, then the protein was eluted with Ni-buffer containing 200 mM imidaziole
407 (Merck) and loaded onto amylose resin (NEB). After washing with amylose-buffer (25 mM
408 sodium phosphate pH 7.8, 150 mM NaCl), the protein was eluted with amylose-buffer con-
409 taining 10 mM maltose. For TEV digest, the fusion protein was incubated overnight at 4°C
410 with 0.27 µg/µL self-made TEV protease, expressed from pRK793 (Addgene, plasmid
411 8827), in 50 mM phosphate pH 8.0, 0.5 mM EDTA, 1 mM DTT and loaded onto a Ni-agarose
412 column (Qiagen) equilibrated with Ni-buffer. The flow-through containing the tag-free X-
413 eK-Flv substrate was concentrated with an Amicon Ultra-15 (Merck Millipore).
414

415 *PRT1 cloning, expression and purification*

416 The coding sequence of *Arabidopsis* PRT1 was cloned according to gene annotations at
417 TAIR (www.arabidopsis.org) from cDNA. The Sequence was flanked by an N-terminal TEV
418 recognition sequence for facilitated downstream purification using the primers ss_prt1_tev
419 (5'-GCTTAGAGAATCTTTATTTTCAGGGGATGGCCGAAACTATGAAAGATATTAC-3') and
420 as_prt1_gw (5'-GGGTATCATTCTGTGCTTGATGACTCATTAG-3'). A second PCR using the
421 primers adapter (5'-GGGGACAAGTTTGTACAAAAAAGCAGGCTTAGAGAATCTTTATTTTCAG
422 GGG-3') and prt1_pos2_as (5'-GGGGACCACTTTGTACAAGAAAGCTGGGTATCATTCTGTGCTT
423 GATGA-3') was performed to amplify the construct to use it in a BP reaction for cloning into
424 pDONR201 (Invitrogen) followed by an LR reaction into the vector pVP16.[52] Recombina-
425 tion into this Gateway destination vector containing a 8xHis:MBP coding sequence 5' of the
426 Gateway cassette leads to an N-terminal 8xHis:MBP double affinity tag.

427 The 8xHis:MBP:PRT1 isolation, cleavage and purification was done as described above for
428 the X-eK-Flv but the Ni-buffer contained 10% glycerol and 0.1% Tween 20.

429

430 ***Chemical labeling***

431 10 μM of purified X-eK-Flv was incubated for 1 h at room temperature with 100 μM of the
432 synthesized thiol reactive fluorogenic labeling dye in 20 mM Tris-Cl pH 8.3, 1 mM EDTA
433 and 1 mM tris(2-carboxy-ethyl)phosphine (TCEP, Thermo Scientific). The reaction was
434 stopped with 1 mM cysteine hydrochloride, the unreactive dye removed using 10 kDa cut-
435 off Amicon filters (Merck Millipore) by three successive washing steps, and the labeling
436 efficiency evaluated by fluorescence intensity of the labeled dye (Tecan M1000) and total
437 protein concentration using infra-red spectroscopy (Direct Detect, Merck Millipore).

438

439 ***Chemical synthesis***

440 The detailed synthesis protocols of the labeling probe NBD-NH-PEG_2-NH-haloacetamide
441 are described in **Supplementary Methods**. In brief, the following synthesis steps were ac-
442 complished: 1) tert-butyl {2-[2-(2-aminoethoxy)ethoxy)ethyl}carbamate (NH_2-PEG_2-
443 NHBoc); 2) NBD-NH-PEG_2-NHBoc; 3) NBD-NH-PEG_2-NH_2 hydrochloride; 4) NBD-NH-PEG_2-
444 NH-iodo-acetamide; 5) NBD-NH-PEG_2-NH-iodoacetamide; 6) NBD-NH-PEG_2-NH-
445 chloroacetamide.

446

447 ***tert*-butyl {2-[2-(2-aminoethoxy)ethoxy)ethyl}carbamate (NH_2-PEG_2-NHBoc)**

448 To a solution of 2,2'-(ethylenedioxy)-bis(ethylamine) (50.00 mL, 33.83 mmol; 495.6
449 %) in dry dioxane (190 mL), di-*tert*-butyl dicarbonate (14.90 g, 68.27 mmol, 100 %) in dry
450 dioxane (60 mL) was added slowly and the resulting mixture was stirred at 25 °C for 12 h.
451 The reaction mixture was filtered, the solvent was removed under reduced pressure and
452 the remaining residue was dissolved in distilled water (300 mL). The aqueous phase was
453 extracted with dichloromethane (3 x 250 mL). Finally, the combined organic phases were
454 dried (Na_2SO_4) and the solvent was removed under reduced pressure to yield *tert*-butyl {2-
455 [2-(2-aminoethoxy)ethoxy)ethyl}carbamate (NH_2-PEG_2-NHBoc) as light yellow oil (16.09 g,
456 64.8 mmol, 94.9 %). ^{1}H NMR (400 MHz; $CDCl_3$) δ: 1.42 (br. s., 2H), 1.42 – 1.46 (m, 9H), 2.87
457 – 2.90 (m, 2H), 3.32 (m, 2H), 3.52 (m, , 2H), 3.55 (m, , 2H), 3.61 – 3.64 (m, 4H), 5.13 (br. s.,
458 1H) ppm; ^{13}C NMR (100 MHz, $CDCl_3$) δ: 28.4, 40.3, 41.8, 67.1, 70.2, 73.5, 79.2, 156.0 ppm;
459 ESI-MS m/z: 248.7 $[M + H]^+$, 497.4 $[2M + Na^+]^+$; HRMS (ESI) calculated for $C_{11}H_{25}N_2O_4$
460 249.1809, found 249.1809.

461

462 **NBD-NH-PEG$_2$-NHBoc**

463 To a suspension of *tert*-butyl {2-[2-(2-aminoethoxy)ethoxy)ethyl}carbamate (1.50 g,
464 6.04 mmol, 100 %) and sodium bicarbonate (1.01 g, 12.08 mmol; 200 %) in acetonitrile (30
465 mL), 4-chloro-7-nitrobenzofurazan (NBD) (1.80 g, 9.06 mmol, 150 %) in acetonitrile (30
466 mL) was added slowly over a period of 2 h and the resulting mixture was stirred at 25 °C
467 for 12 h. The reaction mixture was filtered, the solvent was removed under reduced pres-
468 sure, and the remaining residue was subjected to chromatography (silica gel, methanol /
469 ethyl acetate, 5 : 95) to yield NBD-NH-PEG$_2$-NHBoc as a brown solid (1.89 g, 4.58 mmol,
470 75.9 %). M.p.: 85 – 86 °C; R_F = 0.56 (methanol / ethyl acetate, 5 : 95); ^{1}H NMR (400 MHz;
471 $CDCl_3$) δ [ppm]: 1.42 – 1.45 (m, 9H), 3.31 – 3.37 (m, 2H), 3.54 – 3.56 (m, 2H), 3.58 – 3.60 (m,
472 2H), 3.61 – 3.71 (m, 4 H), 3.87 (m, 2H), 5.02 (m, 1H), 6.20 (d, *J* = 8.6 Hz, 1H) , 6.88 (m, 1H),
473 8.49 (d, *J* = 8.6 Hz, 1H); ^{13}C NMR (100 MHz; $CDCl_3$) δ [ppm]: 28.4, 43.6, 68.1, 70.2, 70.2, 70.4,
474 70.5, 77.2, 98.7, 136.3, 143.9, 144.0, 144.0, 144.3, 155.9; ESI-MS m/z: 410.5 $[M - H]^+$, 434.2
475 $[M + Na]^+$, 845.4 $[2M + Na]^+$; HRMS (ESI) calculated for $C_{17}H_{25}N_5O_7Na$ 434.1646, found
476 434.1647.

477

478 **NBD-NH-PEG$_2$-NH$_2$ hydrochloride**

479 To a solution of NBD-NH-PEG$_2$-NHBoc (2.08 g, 5.06 mmol, 100 %) in dry methanol
480 (20 mL), trimethylsilyl chloride (2.70 mL, 21.27 mmol, 500 %) was added *via* syringe and
481 the resulting mixture was stirred at 25 °C for 12 h. The solvent was removed under re-
482 duced pressure. The remaining residue was suspended in diethyl ether (15 mL), filtered
483 and the solid was washed with several portions of diethyl ether, and the remaining solid

484 was dried under reduced pressure to yield NBD-NH-PEG_2-NH_2 hydrochloride as a brown
485 solid (1.56 g, 5.01 mmol, 98.9 %). The crude product was used without further purification.
486 M.p.: 192 – 193 °C; ^{1}H NMR (400 MHz; CD_3OD) δ [ppm]: 3.09 – 3.11 (m, 2H), 3.64 – 3.76 (m,
487 8H), 3.87 – 3.90 (m, 2 H), 6.19 (d, *J* = 8.4 Hz, 1H), 8.45 (d, *J* = 8.7 Hz, 1H); ^{13}C NMR (100
488 MHz; CD_3OD) δ [ppm]: 41.5, 41.7, 70.1, 70.3, 70.8, 73.2, 98.8, 123.0, 136.5, 144.1, 144.4,
489 144.8; ESI-MS m/z: 310.5 $[M - 2H]^+$, 312.3 $[M]^+$; HRMS (ESI) calculated for $C_{12}H_{18}N_5O_5$
490 312.1303, found 312.1303.
491

492 **NBD-NH-PEG_2-NH-iodoacetamide**

493 To a solution of NBD-NH-PEG_2-NH_2 hydrochloride (202.3 mg, 0.65 mmol; 100 %)
494 and *N*,*N*'-diisopropylethylamine (134.3 µL, 0.77 mmol, 120 %) in dry acetonitril (4.0 mL),
495 iodoacetic anhydride (401.0 mg, 1.13 mmol; 174 %) was added slowly and the resulting
496 mixture was stirred at 25 °C for 12 h. The solvent was removed under reduced pressure
497 and the remaining residue was subjected to chromatography (silica gel, methanol / ethyl
498 acetate, 10 : 90) to yield NBD-NH-PEG_2-NH-iodoacetamide as a brown solid (151.1 mg, 0.32
499 mmol, 48.5 %). R_F = 0.45 (methanol / ethyl acetate, 10 : 90); ^{1}H NMR (400 MHz; $CDCl_3$) δ
500 [ppm]: 3.50 – 3.54 (m, 2H), 3.62 – 3.65 (m, 2H), 3.69 – 3.71 (m, 8H), 3.73 – 3.76 (m, 2H),
501 6.21 (d, *J* = 8.7 Hz, 1H), 6.55 (br. s., 1H), 6.95 (br. s., 1H), 8.48 (d, J = 8.6 Hz, 1H); ^{13}C NMR
502 (100 MHz; $CDCl_3$) δ [ppm]: 0.56, 40.1, 43.6, 68.1, 69.4, 70.3, 70.5, 136.4, 143.9, 144.3, 167.1;
503 ESI-MS m/z: 478.3 $[M - H]^+$, 502.1 $[M + Na]^+$ + 981.3 $[2M + Na]^+$; HRMS (ESI (negative mo-
504 dus)) calculated for $C_{14}H_{17}N_5O_6I$ 478.0229, found 478.0222.
505

506 **NBD-NH-PEG_2-NH-chloroacetamide**

507 To a solution of NBD-NH-PEG$_2$-NH$_2$ hydrochloride (202.5 mg, 0.65 mmol; 100 %)
508 and *N*,*N*'-diisopropylethylamine (134.3 µL, 0.77 mmol, 120 %) in dry acetonitril (4.0 mL),
509 chloroacetic anhydride (221.7 mg, 1.30 mmol; 200 %) was added slowly and the resulting
510 mixture was stirred at 25 °C for 12 h. The solvent was removed under reduced pressure
511 and the remaining residue was subjected to chromatography (silica gel, methanol / ethyl
512 acetate, 10 : 90) to yield NBD-NH-PEG$_2$-NH-chloroacetamid as a brown solid (150.5 mg,
513 0.39 mmol, 59.7 %). R_F = 0.46 (methanol / ethyl acetate, 10 : 90); ^{1}H NMR (400 MHz; CDCl$_3$)
514 δ [ppm]: 3.54 – 3.58 (m, 2H), 3.64 – 3.75 (m, 8H), 3.87 – 3.90 (m, 2H), 4.06 (m, 2H), 6.20 (d,
515 *J* = 8.7 Hz, 1H), 6.90 (br. s., 1H), 6.98 (br. s., 1H), 8.48 (d, *J* = 8.6 Hz, 1H); ^{13}C NMR (100
516 MHz; CDCl$_3$) δ [ppm]: 30.51, 42.7, 43.6, 68.1, 69.5, 70.3, 70.5, 136.3, 143.9, 144.3, 166.0;
517 ESI-MS m/z: 386.1 [M – H]$^+$, 410.1 [M + Na]$^+$; HRMS (ESI (negative modus)) calculated for
518 $C_{14}H_{17}N_5O_6Cl$ 386.0873, found 386.0863.
519

520 ***Ubiquitination assay and in-gel fluorescence detection***

521 3.4 µM (calculated according to the unlabelled protein) of the X-eK-Flv fluorescently la-
522 beled substrate (X-eK-Flv-NBD) were solved in 25 mM Tris-Cl pH 7.4, 50 mM KCl, 5 mM
523 MgCl$_2$, 0.7 mM DTT containing 16 µM Ubiquitin from bovine erythrocytes (Sigma-Aldrich,
524 U6253). For ubiquitination, 2 mM of ATP (New England Biolabs), 40 nM of E1[15], 0.31 µM of
525 E2 (UBC8)[15], and 5 nM of E3 (8xHis:MBP-tagged or untagged PRT1) were added to the pre-
526 vious mix in a final volume of 30 µL and incubated at 30°C for 1 h. The reaction was
527 stopped by adding 5X reductive SDS-PAGE loading buffer and incubating for 10 min at 96
528 °C followed by SDS-PAGE. The gels were scanned using fluorescence detection on a Ty-
529 phoon FLA 9500 biomolecular imager (GE Healthcare) with a blue excitation laser (473

530 nm) LD and an LBP emission filter (510LP), then blotted onto a cellulose membrane and
531 detected with either mouse monoclonal anti-Ubiquitin antibody (Ub (P4D1), sc-8017, Santa
532 Cruz Biotechnology, 1:5,000 dilution in blocking solution [150 mM NaCl, 10 mM Tris-Cl pH
533 8, 3% skim milk powder, 0.1% Tween 20]) or mouse monoclonal anti-HA epitope tag anti-
534 body (HA.11, clone 16B12: MMS-101R, Covance; 1:1,000 to 1:5,000, in blocking solution)
535 and goat anti-mouse IgG-HRP (1858415, Pierce; 1:2,500 to 1:5,000 dilution in blocking so-
536 lution). The acquired images of the gels (prior blotting) were analyzed using the Gel Ana-
537 lyser densitometric soft (Gel.Analyser.com). Thus, one may use the same gel for both in-gel
538 fluorescence detection followed by blotting and immunodetection.
539 The same gels that were detected via fluorescence scanning were blotted and detected with
540 ECL without further processing such as stripping. Thus, fluorescent detection can be com-
541 bined with ECL in one simple workflow. For evaluation of pH dependence, 50 mM Tris-Cl
542 was used as a buffering agent at pH 6.75, 7.0, 7.5, 8.0, 8.5 and 9.0.
543

544 ***Real-time ubiquitination assay using fluorescence polarization***

545 For fluorescence polarization (FP), the reaction mixture (24 μL) containing all the compo-
546 nents except the ATP was incubated in a 384 well microplate (Corning, Cat. No. 3712 or
547 3764) at 30°C in a M1000 infinite plate reader (Tecan) until the temperature was stable
548 (typically 4-5 min) and the reaction triggered by adding 6 uL of 10 mM ATP preheated to
549 30°C. FP was monitored every 2 min at 562 nm while the excitation wavelength was set to
550 470 nm. The M1000 fluorescence polarization module was calibrated using 10 nM fluores-
551 cein in 10 mM NaOH at P = 20 mP.
552

553 ***Structure modeling of the artificial substrate***

554 The amino acid sequence of the artificial F-eK-Flv substrate was submitted to the Protein
555 Homology/Analogy Recognition Engine V 2.0[53] (Phyre[2], Structural Bioinformatics Group,
556 Imperial College, London) in both normal and intensive modes. The bests selected tem-
557 plates were found to be PBD ID: 3EDC for the eK region and 2M6R for the Flv part) and the
558 model was visualized using ViewerLite (Accelrys Inc.).

559

560 **ACKNOWLEDGEMENTS**

561 We thank Marco Trujillo for expression clones of His:UBC8 and His:UBA1, discussions and
562 constant support in ubiquitination-related issues and Angela Schaks for synthesis of the
563 chemical probe. This work was supported by a grant for setting up the junior research
564 group of the *ScienceCampus Halle – Plant-based Bioeconomy* to N.D., by the grant WE
565 1467/13-1 of the German Research Foundation (Deutsche Forschungsgemeinschaft, DFG)
566 to B.W. funding E.P., a grant of the Leibniz-DAAD Research Fellowship Programme by the
567 Leibniz Association and the German Academic Exchange Service (DAAD) to A.C.M. and N.D.,
568 and Ph.D. fellowships of the Landesgraduiertenförderung Sachsen-Anhalt awarded to C.N.
569 and F.F. Financial support came from the Leibniz Association, the state of Saxony Anhalt,
570 the Deutsche Forschungsgemeinschaft (DFG) Graduate Training Center GRK1026 "*Confor-*
571 *mational Transitions in Macromolecular Interactions*" at Halle, and the Leibniz Institute of
572 Plant Biochemistry (IPB) at Halle, Germany. To complete work on this project, a Short Term
573 Scientific Mission (STSM) of the European Cooperation in Science and Technology (COST,
574 www.cost.eu) was granted to A.C.M. and N.D. by the COST Action BM1307 – "*European net-*
575 *work to integrate research on intracellular proteolysis pathways in health and disease (PRO-*

576 *TEOSTASIS)*". This work was partially funded by the grant DI 1794/3-1 of the German Re-
577 search Foundation to N.D.

578

579 **AUTHOR CONTRIBUTIONS**

580 A.C.M. performed the ubiquitination reactions and related analysis. E.P. and B.W. designed
581 and synthesized the fluorescent probe, B.W. supervised the chemical synthesis, M.K. estab-
582 lished PRT1 ubiquitination reactions, C.N. cloned and purified PRT1, F.F. cloned the X-eK-
583 HAT fragment and performed site-directed mutagenesis. N.D. and A.C.M. designed the
584 study, wrote the manuscript and designed the figures. All authors read and approved the
585 final version of this manuscript.

586 **SUPPLEMENTARY INFORMATION**

587

588 **SUPPLEMENTARY FIGURES**

589 **Supplementary Figure 1. Modeled structure of the F-eK-Flv substrate and PRT1 N-**

590 **terminal specificity.**

591

592 **SUPPLEMENTARY TABLES**

593 **Supplementary Table 1. Oligonucleotides used in this study.**

594

595 **SUPPLEMENTARY METHODS**

596 **Synthesis of the chemical probe NBD-NH-PEG$_2$-NH-haloacetamide.**

597 **REFERENCES**

598

599 1. Bachmair A, Becker F, Schell J. Use of a reporter transgene to generate arabidopsis mutants in
600 ubiquitin-dependent protein degradation. *Proc Natl Acad Sci U S A* **90**, 418-421 (1993).
601
602 2. Potuschak T, Stary S, Schlogelhofer P, Becker F, Nejinskaia V, Bachmair A. PRT1 of Arabidopsis
603 thaliana encodes a component of the plant N-end rule pathway. *Proc Natl Acad Sci U S A* **95**,
604 7904-7908 (1998).
605
606 3. Stary S, Yin X, Potuschak T, Schlogelhofer P, Nizhynska V, Bachmair A. PRT1 of Arabidopsis is a
607 ubiquitin protein ligase of the plant N-end rule pathway with specificity for aromatic amino-
608 terminal residues. *Plant Physiol* **133**, 1360-1366 (2003).
609
610 4. Bachmair A, Finley D, Varshavsky A. In vivo half-life of a protein is a function of its amino-
611 terminal residue. *Science* **234**, 179-186 (1986).
612
613 5. Varshavsky A. The N-end rule pathway and regulation by proteolysis. *Protein Sci* **20**, 1298-1345
614 (2011).
615
616 6. Dougan D, Truscott K, Zeth K. The bacterial N-end rule pathway: expect the unexpected. *Mol*
617 *Microbiol* **76**, 545-558 (2010).
618
619 7. Tasaki T, Sriram S, Park K, Kwon Y. The N-end rule pathway. *Annu Rev Biochem* **81**, 261-289
620 (2012).
621
622 8. Gibbs DJ. Emerging Functions for N-Terminal Protein Acetylation in Plants. *Trends Plant Sci* **20**,
623 599-601 (2015).
624
625 9. Gibbs DJ, Bacardit J, Bachmair A, Holdsworth MJ. The eukaryotic N-end rule pathway: conserved
626 mechanisms and diverse functions. *Trends Cell Biol* **24**, 603-611 (2014).
627
628 10. Zenker M*, et al.* Deficiency of UBR1, a ubiquitin ligase of the N-end rule pathway, causes
629 pancreatic dysfunction, malformations and mental retardation (Johanson-Blizzard syndrome).
630 *Nat Genet* **37**, 1345-1350 (2005).
631
632 11. Piatkov K, Brower C, Varshavsky A. The N-end rule pathway counteracts cell death by destroying
633 proapoptotic protein fragments. *Proc Natl Acad Sci U S A* **109**, E1839-1847 (2012).
634
635 12. Brower C, Piatkov K, Varshavsky A. Neurodegeneration-associated protein fragments as short-
636 lived substrates of the N-end rule pathway. *Mol Cell* **50**, 161-171 (2013).
637
638 13. Shemorry A, Hwang C, Varshavsky A. Control of protein quality and stoichiometries by N-
639 terminal acetylation and the N-end rule pathway. *Mol Cell* **50**, 540-551 (2013).
640
641 14. Kim H, Kim R, Oh J, Cho H, Varshavsky A, Hwang C. The N-Terminal Methionine of Cellular
642 Proteins as a Degradation Signal. *Cell* **156**, 158-169 (2014).
643

15. Gibbs DJ*, et al.* Homeostatic response to hypoxia is regulated by the N-end rule pathway in plants. *Nature* **479**, 415-418 (2011).

16. Licausi F*, et al.* Oxygen sensing in plants is mediated by an N-end rule pathway for protein destabilization. *Nature* **479**, 419-422 (2011).

17. Gibbs D*, et al.* Nitric Oxide Sensing in Plants Is Mediated by Proteolytic Control of Group VII ERF Transcription Factors. *Mol Cell* **53**, 369-379 (2014).

18. Weits D*, et al.* Plant cysteine oxidases control the oxygen-dependent branch of the N-end-rule pathway. *Nat Commun* **5**, 3425 (2014).

19. Mendiondo GM*, et al.* Enhanced waterlogging tolerance in barley by manipulation of expression of the N-end rule pathway E3 ligase PROTEOLYSIS6. *Plant Biotechnol J* **14**, 40-50 (2016).

20. de Marchi R*, et al.* The N-end rule pathway regulates pathogen responses in plants. *Sci Rep* **6**, 26020 (2016).

21. Holman T*, et al.* The N-end rule pathway promotes seed germination and establishment through removal of ABA sensitivity in Arabidopsis. *Proc Natl Acad Sci U S A* **106**, 4549-4554 (2009).

22. Abbas M*, et al.* Oxygen sensing coordinates photomorphogenesis to facilitate seedling survival. *Curr Biol* **25**, 1483-1488 (2015).

23. Gibbs DJ, Conde JV, Berckhan S, Prasad G, Mendiondo GM, Holdsworth MJ. Group VII Ethylene Response Factors Coordinate Oxygen and Nitric Oxide Signal Transduction and Stress Responses in Plants. *Plant Physiol* **169**, 23-31 (2015).

24. Graciet E*, et al.* The N-end rule pathway controls multiple functions during Arabidopsis shoot and leaf development. *Proc Natl Acad Sci U S A* **106**, 13618-13623 (2009).

25. Yoshida S, Ito M, Callis J, Nishida I, Watanabe A. A delayed leaf senescence mutant is defective in arginyl-tRNA:protein arginyltransferase, a component of the N-end rule pathway in Arabidopsis. *Plant J* **32**, 129-137 (2002).

26. Schuessele C*, et al.* Spatio-temporal patterning of arginyl-tRNA protein transferase (ATE) contributes to gametophytic development in a moss. *New Phytol* **209**, 1014-1027 (2016).

27. Hoernstein SN*, et al.* Identification of targets and interaction partners of arginyl-tRNA protein transferase in the moss Physcomitrella patens. *Mol Cell Proteomics*, (2016).

28. Faden F*, et al.* Phenotypes on demand via switchable target protein function in multicellular organisms. *Nat Commun* **in press**, (accepted pending minor revision).

29. Sriram S, Kim B, Kwon Y. The N-end rule pathway: emerging functions and molecular principles of substrate recognition. *Nat Rev Mol Cell Biol* **12**, 735-747 (2011).

691 30. Venne AS, Solari FA, Faden F, Paretti T, Dissmeyer N, Zahedi RP. An improved workflow for
692 quantitative N-terminal charge-based fractional diagonal chromatography (ChaFRADIC) to study
693 proteolytic events in Arabidopsis thaliana. *Proteomics* **15**, 2458-2469 (2015).
694
695 31. Tsiatsiani L*, et al.* The Arabidopsis metacaspase9 degradome. *Plant Cell* **25**, 2831-2847 (2013).
696
697 32. Humbard M, Surkov S, De Donatis G, Jenkins L, Maurizi M. The N-degradome of escherichia coli:
698 limited proteolysis in vivo generates a large pool of proteins bearing N-degrons. *J Biol Chem* **288**,
699 28913-28924 (2013).
700
701 33. Apel W, Schulze W, Bock R. Identification of protein stability determinants in chloroplasts. *Plant*
702 *J* **63**, 636-650 (2010).
703
704 34. Garzón M*, et al.* PRT6/At5g02310 encodes an Arabidopsis ubiquitin ligase of the N-end rule
705 pathway with arginine specificity and is not the CER3 locus. *FEBS Lett* **581**, 3189-3196 (2007).
706
707 35. Kumar E, Charvet C, Lokesh G, Natarajan A. High-throughput fluorescence polarization assay to
708 identify inhibitors of Cbl(TKB)-protein tyrosine kinase interactions. *Anal Biochem* **411**, 254-260
709 (2011).
710
711 36. Smith M*, et al.* The E3 ubiquitin ligase CHIP and the molecular chaperone Hsc70 form a dynamic,
712 tethered complex. *Biochemistry* **52**, 5354-5364 (2013).
713
714 37. Xia Z, Webster A, Du F, Piatkov K, Ghislain M, Varshavsky A. Substrate-binding sites of UBR1, the
715 ubiquitin ligase of the N-end rule pathway. *J Biol Chem* **283**, 24011-24028 (2008).
716
717 38. Kapust R, Tozser J, Copeland T, Waugh D. The P1' specificity of tobacco etch virus protease.
718 *Biochem Biophys Res Commun* **294**, 949-955 (2002).
719
720 39. Phan J*, et al.* Structural basis for the substrate specificity of tobacco etch virus protease. *J Biol*
721 *Chem* **277**, 50564-50572 (2002).
722
723 40. Naumann C, Mot A, Dissmeyer N. Generation of artificial N-end rule substrate proteins in vivo
724 and in vitro. *Methods Mol Biol*, (in press).
725
726 41. Stegmann M*, et al.* The ubiquitin ligase PUB22 targets a subunit of the exocyst complex required
727 for PAMP-triggered responses in Arabidopsis. *Plant Cell* **24**, 4703-4716 (2012).
728
729 42. Sadowski M, Sarcevic B. Mechanisms of mono- and poly-ubiquitination: Ubiquitination
730 specificity depends on compatibility between the E2 catalytic core and amino acid residues
731 proximal to the lysine. *Cell Div* **5**, 19 (2010).
732
733 43. Lu Y, Wang W, Kirschner MW. Specificity of the anaphase-promoting complex: a single-molecule
734 study. *Science* **348**, 1248737 (2015).
735
736 44. Petroski MD, Deshaies RJ. Mechanism of lysine 48-linked ubiquitin-chain synthesis by the cullin-
737 RING ubiquitin-ligase complex SCF-Cdc34. *Cell* **123**, 1107-1120 (2005).
738

739 45. Deshaies RJ, Joazeiro CA. RING domain E3 ubiquitin ligases. *Annu Rev Biochem* **78**, 399-434
740 (2009).
741
742 46. Bachmair A, Varshavsky A. The degradation signal in a short-lived protein. *Cell* **56**, 1019-1032
743 (1989).
744
745 47. Melvin A, Woss G, Park J, Dumberger L, Waters M, Allbritton N. A comparative analysis of the
746 ubiquitination kinetics of multiple degrons to identify an ideal targeting sequence for a
747 proteasome reporter. *PLoS One* **8**, e78082 (2013).
748
749 48. Ronchi VP, Haas AL. Measuring rates of ubiquitin chain formation as a functional readout of
750 ligase activity. *Methods Mol Biol* **832**, 197-218 (2012).
751
752 49. Berndsen CE, Wolberger C. New insights into ubiquitin E3 ligase mechanism. *Nat Struct Mol Biol*
753 **21**, 301-307 (2014).
754
755 50. Plechanovova A, Jaffray EG, Tatham MH, Naismith JH, Hay RT. Structure of a RING E3 ligase and
756 ubiquitin-loaded E2 primed for catalysis. *Nature* **489**, 115-120 (2012).
757
758 51. Ye Y, Rape M. Building ubiquitin chains: E2 enzymes at work. *Nat Rev Mol Cell Biol* **10**, 755-764
759 (2009).
760
761 52. Thao S*, et al.* Results from high-throughput DNA cloning of Arabidopsis thaliana target genes
762 using site-specific recombination. *J Struct Funct Genomics* **5**, 267-276 (2004).
763
764 53. Kelley LA, Mezulis S, Yates CM, Wass MN, Sternberg MJ. The Phyre2 web portal for protein
765 modeling, prediction and analysis. *Nat Protoc* **10**, 845-858 (2015).
766
767